VULNERABILITY OF SPACECRAFT NICKEL-CADMIUM BATTERIES TO HYPERVELOCITY IMPACTS

Robin Putzar[(1)] **and Frank Schäfer**[(2)]

[(1)] *Fraunhofer EMI, Ernst-Zermelo-Str. 4, 79104 Freiburg, Germany, robin.putzar@emi.fraunhofer.de*
[(2)] *Fraunhofer EMI, Ernst-Zermelo-Str. 4, 79104 Freiburg, Germany, frank.schaefer@emi.fraunhofer.de*

ABSTRACT

During a study performed in framework of a European Space Agency contract, the vulnerability of space-grade nickel cadmium batteries was assessed. The batteries were shielded by representative aluminum honeycomb sandwich panels covered by multi-layer insulation. Four hypervelocity impact tests on battery cells and three tests on battery cell casings were performed. Impact direction was the surface normal in all tests. Impact velocities range between 6.3 and 6.8 km/s, projectiles were single spheres made of 99.9 % pure aluminum having diameters between 2.5 and 6.0 mm.

The batteries were charged prior the tests. During the tests, the batteries were connected to a resistor simulating an electric load, with the voltage across the resistor being monitored by an oscilloscope. After the tests, the electrical capacity of the cells was investigated again.

The tests showed that failure of the cells can be related to the mechanical damage to the casing. Non-perforated cells showed no sign of performance degradation. Small perforation holes in the cell walls caused very short (up to ca. 100 μs) voltage drops and lead to a slightly decreased cell voltage in some cases, but not in all. One cell was perforated so heavily that its voltage dropped to 10 % of the original value within approx. 30 s, and dropped to effectively zero after that. Cell capacity was only measured shortly after the impact tests. However, it is assumed that successive full charge-discharge cycles of the cell would lead to complete loss of electrical capacity, because of the catalytic fluid evaporating gradually through the small impact hole(s) from the pressure build-up in the cell in a charged state. Therefore it is assumed that perforated cells will gradually fail post impact.

Even for a quite high impact energy resulting in complete failure of the battery during test, the failing cell did neither explode nor cause other damage to an adjacent cell.

Figure 1. Nickel cadmium battery cell after hypervelocity impact (exp. 4763).

Keywords: nickel cadmium batteries; hypervelocity impact; vulnerability assessment.

1. INTRODUCTION

Space debris and meteoroid protection requirements for spacecraft are often formulated in terms of probability of no penetration (PNP) of the structure wall. For manned pressurized modules, this is justified by safety and operational considerations taking into account the presence of crew onboard.

The perforation of an unmanned spacecraft's external structure does not necessarily endanger the mission, since the mechanical strength of the structure is not a concern when in orbit. An exception is the case of exposed key equipment such as pressure vessels, for which an impact-induced burst will lead to termination of the mission as well as contribute to space debris generation and pollution of key orbits.

Since a spacecraft's key equipment is often located behind a structure wall, a more favorable approach is to evaluate the risk of functional damage to such equipment, as is possible with advanced software tools like EMI's PIRAT [1]. The so-defined equipment vulnerability is a function of the threat posed by the meteoroid/debris environment and the spacecraft configuration.

A comprehensive look at the vulnerability of different spacecraft subsystems is necessary to define the limit between tolerable damage and failure. During a study performed in framework of a European Space Agency contract, several types of key equipment were identified [2]: pressure vessels (oxidizer and fuel tanks, pressurant tanks), pipes (fuel pipes and heat pipes), harnesses, and on board data handling. To investigate the respective vulnerability of this equipment, hypervelocity impact tests were performed [3, 4, 5]. This publication addresses the results obtained for nickel-cadmium batteries.

Figure 2. Photograph of one battery sample tested.

2. EXPERIMENTAL METHOD

Four hypervelocity impact tests on shielded nickel-cadmium battery cells were performed. To account for typical on-board configurations, the cells were placed behind an Al (aluminum) H/C (honeycomb) SP (sandwich panel) structure wall with MLI (multi-layer thermal insulation) attached outside. Additionally, three hypervelocity impact tests on shielded battery casing walls were performed to pre-evaluate the ballistic perforcmance of the battery casing.

The impact tests were performed at Fraunhofer EMI's Space Gun. The tests on battery casing walls were performed in December 2004, the tests on the batteries were performed in November 2005.

The battery cells used are identical to space grade hardware. They are of type SAFT VOS 40 AGBC. Manufacturer of the cells is SAFT. Their nameplate capacity is 40 Ah. The cell wall consists of 0.4 mm thick stainless steel (AISI 304L, 7.9 g/cm^3). Figure 2 shows a photograph of a battery.

The structure wall was selected based on the specification for the MetOp satellite structure wall. The face sheets are 0.41 mm (0.016 in) thick and consist of Al 2024 T3 (2.76 g/cm^3). The specification of the 35 mm thick H/C core is 2.0-3/16-07P-5056-MIL-C-7438G. The actual sandwich panel thickness was 38.9 $\pm$ 0.1 mm in all experiments. Figure 3 shows a photograph of a sample of the sandwich panel.

MLI with an areal density of 0.447 kg/m^2 was used. The layup is (from outside to inside): 1 layer beta cloth 500 GW, 8 layers of 0.3 mil perforated Kapton with VDA (vapor deposited Al) on both sides, 1 layer of 1.0 mil perforated Kapton with VDA on the

Figure 3. Photograph of aluminum honeycomb sandwich panel used to shield the batteries.

inside. Between every two layers, a Dacron spacer net was placed. The average thickness of the unstressed MLI was approx. 2.0 $\pm$ 0.5 mm. When gently pressed together the thickness of the MLI was approx. 0.8 $\pm$ 0.2 mm.

The spacing between the Al H/C SP and the battery front side (or battery casing front side, respectively) was 100 mm in all tests. Two of the tests on casing material only were performed without MLI, all others were performed with MLI.

For the tests with battery cell walls only, two witness plates made of 1.0 mm thick Al 2024 T351 (3.1364.T351) were placed behind the battery cell wall. The spacing between the cell wall and the first witness plate was 50 mm, the spacing between the two witness plates was 20 mm.

Figures 4 and 5 show sketches of the set-up. Figure 6 shows an example photograph of the set-up. Figure 7 shows the battery placed inside the target chamber, showing the protective casing to prevent contamination of the target chamber.

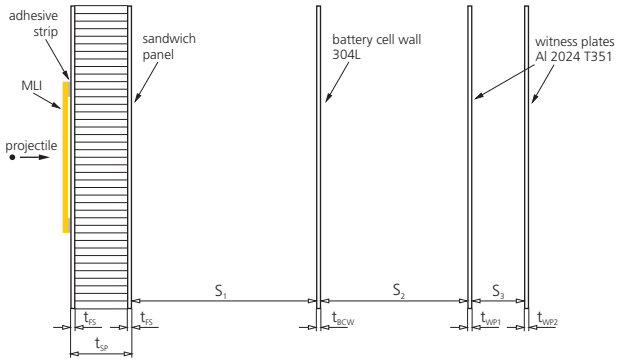

Figure 4. Sketch of test set-up with battery casing walls.

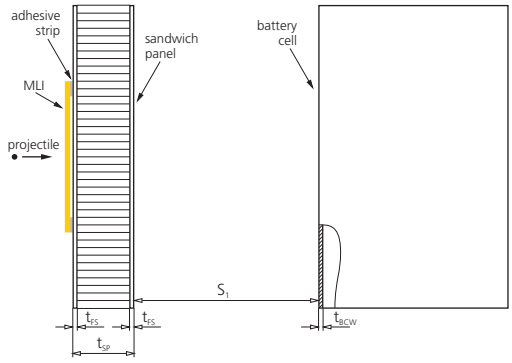

Figure 5. Sketch of test set-up with space-grade batteries.

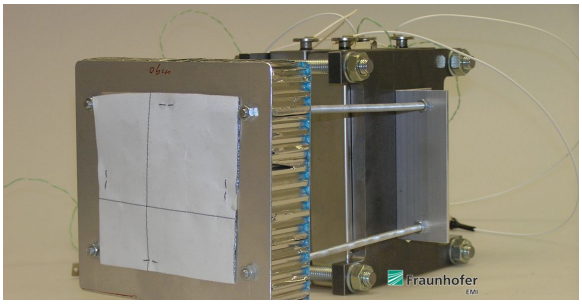

Figure 6. Photograph of test set-up of experiment 4763.

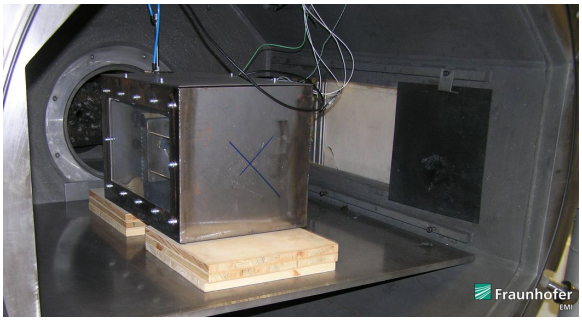

Figure 7. Photograph of battery in container prior experiment 4762.

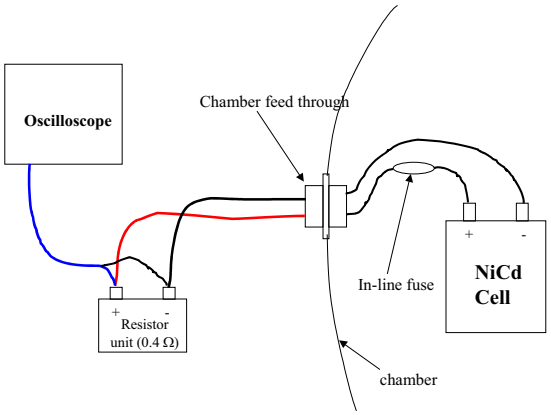

Figure 8. Sketch of the electrical set-up.

The batteries were charged prior the tests, but not to full capacity. During the test, they were connected to a 0.33 Ω resistor to simulate an electrical load, except for experiment 4762, where a 0.22 Ω resistor was used. The resistor was situated outside the target chamber. The voltage drop across the resistor was measured using an oscilloscope. Figure 8 shows a sketch of the electrical setup.

Aluminum spheres with diameters between 2.5 and 6.0 mm were used as impactors. Impact velocity was targeted at around 6.5 km/s. All projectiles were made of 99.9 % aluminum. All impacts were with respect to the surface normal.

3. EXPERIMENTAL RESULTS

All tests were performed around 6.5 km/s with the projectile diameter (i.e. projectile mass) being varied to generate different impact loads. In the configuration tested, the projectile diameter leading to perforation of the battery casing wall is between 2.5 and 3.5 mm. Table 1 shows a summary of all tests performed.

Detailed damage descriptions

In exp. 4604, the battery cell wall was not perforated. Instead, the wall features some bulges, the depth of the deepest bulge was 1.4 mm. There was no damage on either witness plate.

In exp. 4598, there were two holes in the battery cell wall. The size of the largest hole was 3.0 ± 0.3 mm $\times$ 2.6 ± 0.3 mm. The first witness plate featured some craters, the second witness plate was not damaged.

In exp. 4596, the battery cell wall was perforated with approx. 35 holes. The size of the largest hole

Table 1. Summary of experiments on battery cells. Exp. – experiment number, S – spacing, v_0 – impact velocity, d_P – projectile diameter, m_P – projectile mass, α – impact angle. Note: Electrical performance is within one hour after test.

Exp.	Target	Structure Wall	S [mm]	v_0 [km/s]	d_P [mm]	m_P [mg]	α [1]	Mechanical Damage	Electrical Performance (see Note)
4604	casing	MLI+SP	100	6.8	2.5	21.3	0°	no perforation	—
4598	casing	SP	100	6.59	3.5	58.8	0°	perforation	—
4596	casing	SP	100	6.33	4.5	124.0	0°	perforation	—
4760	1 cell	MLI+SP	100	6.37	2.5	21.2	0°	no perforation	nominal
4761	1 cell	MLI+SP	100	6.71	3.5	62.1	0°	perforation	nominal
4762	2 cells	MLI+SP	100	6.53	4.5	123.8	0°	1: no perforation	1: nominal
								2: perforation	2: nominal
4763	2 cells	MLI+SP	100	6.42	6.0	297.5	0°	1: perforation	1: nominal
								2: perforation	2: failed

was 3.0 mm × 2.9 mm. The first witness plate featured two holes, and there were few small craters on the second witness plate.

In exp. 4760, the battery cell wall was not perforated. The depth of the deepest crater was 1.1 mm. The battery cell function was nominal during and up to one hour after impact testing.

In exp. 4761, the battery cell wall was perforated. There were two holes. The size of the largest hole was ca. 1.1 ± 0.2 mm in diameter. The battery cell function was nominal during and up to one hour after impact testing.

In exp. 4762, cell 1 was not perforated. The depth of the deepest crater in cell 1 was 0.4 mm. Cell 2 was perforated. The size of the largest hole in cell 2 was 0.7 ± 0.2 mm × 0.9 ± 0.2 mm. Both cells were functioning nominally during and up to one hour after impact testing.

In exp. 4763, cell 1 was perforated with ca. 21 holes. The size of the largest hole in cell 1 was 1.5×2.0 mm. Cell 2 was perforated with approx. 25 holes. The size of the largest perforation hole in cell 2 was 14 mm × 9 mm. The function of cell 1 was nominal during and up to one hour after impact testing. Cell 2 failed during the test; the cell voltage dropped to half its original value within 6.3 s. The cell lost its entire capacity within 120 seconds after the impact. The voltage of both cells dropped during the initial 250 μs after the impact by approx. 250 mV.

Figures 9 to 11 show the battery front sides after test.

Figure 9. Mechanical damage to battery front side in experiments 4760 (left) and 4761 (right).

Figure 10. Mechanical damage to battery front side in experiments 4762.

Figure 11. Mechanical damage to battery front side in experiments 4763.

Electrical performance

Figures 12 to 17 show the electrical performance of the batteries in the experiments.

All signals show a peak approx. 45 to 50 μs before the impact flash trigger that was determined to be related to the power supply of the Xenon flash lamp for the high speed camera back-light illumination. The peaks at time of projectile impact on the SP are presumably caused by plasma emissions that induced voltage peaks on the cables that were connected to the cells. It is noted that the cables used to connect to the batteries were not electrically shielded.

The signals recorded during experiments 4760 and 4761 (figures 12 and 13) show no effect of the impact on the battery voltage during the initial 360 μs after impact. The reason for a peak approx. 88 μs after impact in experiment 4761 is unknown; no correlation between the impact event could be identified. In experiment 4760, the cell voltage remained constant, indicating nominal cell function. In experiment 4761, which caused cell wall perforation, the cell voltage was not altered for at least 60 minutes after the test. This cell was discharged through a resistor at a later stage. During the capacity checks performed during post-impact characterization, it was found that the capacity was not altered measurably, noting however that the level of charging for the post-impact function assessments was just about 10 % of the maximum charge the battery can contain. It is assumed that successive full charge-discharge cycles of the cell would lead to complete loss of electrical capacity, because of the catalytic fluid evaporating gradually through the small impact hole from the pressure build-up in the cell in a charged state.

The signals recorded during experiment 4762 (figures 14 and 15) show some effect during impact: a peak at the time the fragment cloud impacts on the battery cells (approx. 30 μs after impact flash trigger). Further, the battery cell that is perforated (no. 772-068), experiences a slight voltage drop of approximately 50 mV (ca. 5 % of nominal cell voltage), lasting for a duration of ca. 30 μs almost immediately after the encounter of the fragment cloud on the cell. After this, the voltage remains stable for at least 2 minutes (end of recording time). In post-test characterization of the perforated battery cell it was shown that the capacity decreased just slightly, however, the same comments as for exp. 4761 apply here.

In experiment 4763, the battery cell voltage was significantly affected during impact (see figures 16 and 17). Both cells experience significant voltage drops of up to 50 % during the initial 250 μs after the impact (approx. 250 mV for both batteries with approx. 320 μs and 70 μs duration for battery no. 771-041 and 772-008, respectively). The voltage of battery no. 771-041 (the heavily perforated) dropped to half its original value within 6.3 s; this cell lost its complete

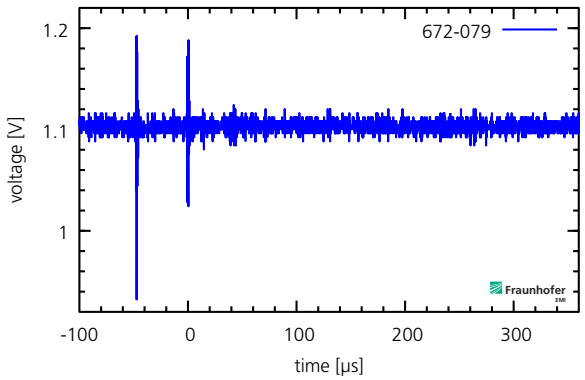

Figure 12. Electrical performance of battery in experiment 4760.

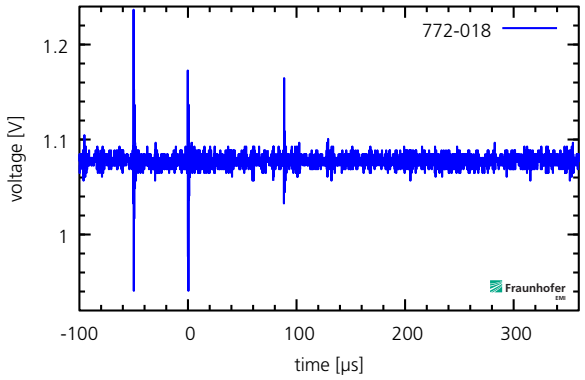

Figure 13. Electrical performance of battery in experiment 4761.

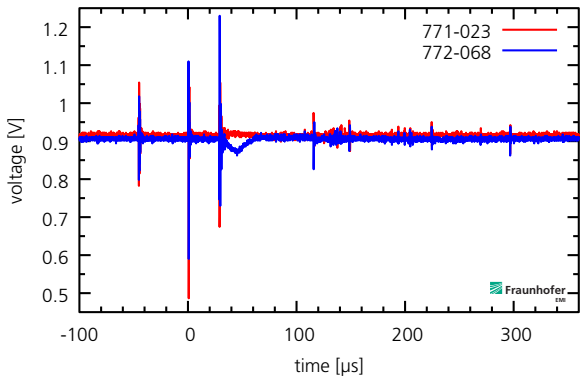

Figure 14. Electrical performance of batteries in experiment 4762. Cell 1 has serial number 771-023, cell 2 has serial number 772-068.

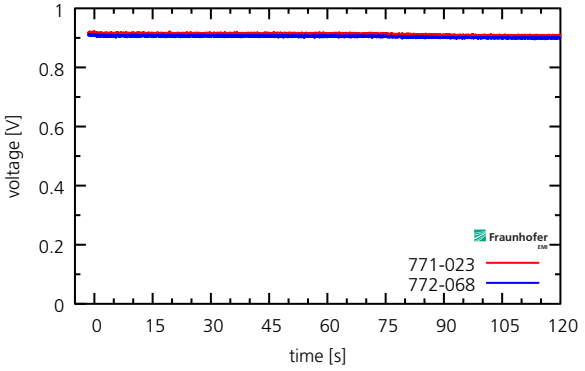

Figure 15. Longer-term electrical performance of batteries in experiment 4762. Cell 1 has serial number 771-023, cell 2 has serial number 772-068.

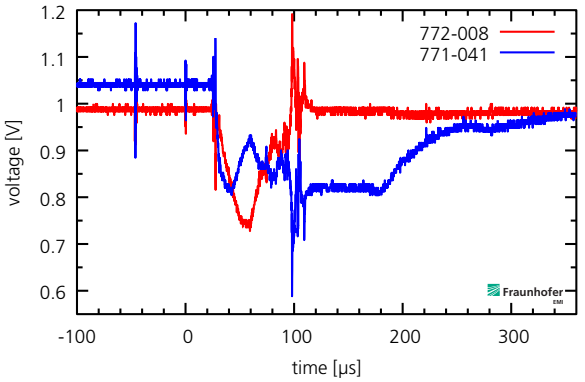

Figure 16. Electrical performance of batteries in experiment 4763. Cell 1 has serial number 772-008, cell 2 has serial number 771-041.

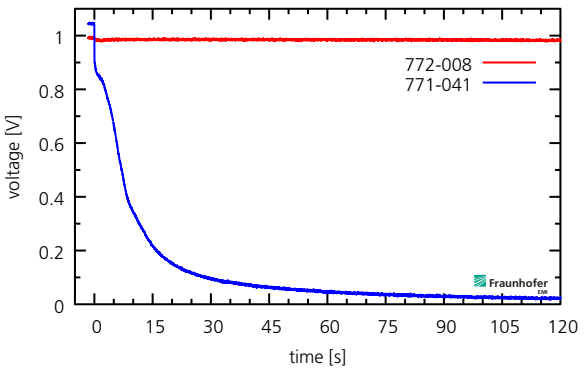

Figure 17. Longer-term electrical performance of batteries in experiment 4763. Cell 1 has serial number 772-008, cell 2 has serial number 771-041.

capacity within 120 seconds after the impact. This indicates a total sudden failure caused by the impact. It is believed that this failure was induced by a short circuit inside the cell, probably due to a large fragment which intruded into the battery. The other cell was analyzed during post-impact characterization of the cell function. As for the other perforated cells it had almost the same residual capacity during the initial charge-discharge cycle compared to before the test, but is expected to fail during subsequent full charge-discharge cycles, see comments above.

4. CONCLUDING REMARKS

The hypervelocity impact tests exhibited two distinct failure modes for shielded nickel cadmium battery cells impacted by micrometeoroids or space debris particles. Both failure modes are related to perforation of the casing wall and material being ejected into the battery.

Lower impact energies, which only cause small perforation holes of the battery casing, will not lead to an instantaneous failure of the battery. Instead, the voltage spikes measured during those impacts may well remain unnoticed, depending on the implementation of the battery cell monitoring. E.g., if only one data point every second (or less) is recorded, no effect can be measured, and there may well be no difference in recording between before and after such an impact event. However, on a longer time scale, such a battery will loose its catalytic fluid, causing a decay in battery performance over time. As charging a battery builds up some internal pressure, charge-discharge-cycles may well contribute to the loss of catalytic fluid. The duration of such a decay will depend on a number of factors, e.g. total hole size in the casing, temperature gradients and the actual charge-discharge-cycle profile.

Higher impact energies, however, which cause a significant amount of matter being placed into the actual battery, can cause immediate malfunction of a nickel-cadmium battery cell. This is most likely caused by short circuits being generated inside the battery, leading to an immediate discharge. The threshold found for this failure mode is between a hole size of 2 and ca. 10 mm. Such an impact should be well noticeable in battery cell monitor recordings.

It should be noted that nickel cadmium batteries are usually not operated alone onboard a spacecraft. Rather, cells are arranged in arrays to achieve the voltage and current capabilities required by the spacecraft. Those set-ups exhibit a certain degree of redundancy, where the destruction of a single cell (or maybe two adjacent cells) might not necessarily lead to a loss of mission.

Another important finding is that even for a quite high impact energy, the failing cell did neither explode nor cause other damage to an adjacent cell.

Destruction of batteries due to particle impacts is a realistic failure scenario. Spacecraft designers may need to take into account failure of single battery cells during mission lifetime. This is especially true for batteries that are not well shielded. Analyses with dedicated software tools [1] can help to determine the actual risk for functional damage.

ACKNOWLEDGMENTS

The impact experiments presented in this paper have been conducted under ESA contract 16483/02.

The support of Hedley Stokes, Jenny Cheese and Richard Chant, at that time working for QinetiQ Ltd Space Department, is greatly appreciated. They contributed substantially to the success of the hypervelocity impact test campaign.

REFERENCES

1. Kempf, S.; Schäfer, F.; Rudolph, M.; Welty, N.; Donath, T.; Destefanis, R.; Grassi, L.; Janovsky, R.; Evans, L.; Winterboer, A.: Risk and vulnerability analysis of satellites due to MM/SD with PIRAT. In: Ouwehand, L. (Ed.): *Proceedings of the 6th European Conference on Space Debris.* Darmstadt, Germany, 2013. ESA SP-723
2. Putzar, R.; Schäfer, F.: *Vulnerability of spacecraft equipment to space debris and meteoroid impacts: Final report: TN5 to ESA contract 16483/02/NL/PA.* Freiburg im Breisgau, Germany: Fraunhofer-Institut für Kurzzeitdynamik, Ernst-Mach-Institut, 2006. EMI Report I-15/06
3. Putzar, R.; Schäfer, F.; Romberg, O.; Lambert, M.: Vulnerability of shielded fuel pipes and heat pipes to hypervelocity impacts. In: Danesy, D. (Ed.): *Proceedings of the 4th European Conference on Space Debris.* Darmstadt, Germany, 2005, pp. 459-464. ESA SP-587
4. Putzar, R.; Schäfer, F.; Stokes, H.; Chant, R.; Lambert, M.: Vulnerability of spacecraft electronics boxes to hypervelocity impacts. In: *Proceedings of the 56th International Astronautical Congress.* Fukuoka, Japan, 2005. IAC-05-B6.4.02
5. Putzar, R.; Schäfer, F.; Lambert, M.: Vulnerability of spacecraft harnesses to hypervelocity impacts. In: *International Journal of Impact Engineering* 35 (2008), pp. 1728-1734. `https://doi.org/10.1016/j.ijimpeng.2008.07.067`